Materials Science Forum
ISSN: 1662-9752, Vol. 1193, pp 25-32
doi:10.4028/p-lQ20LA

Submitted: 2025-09-12
Revised: 2025-12-19
Accepted: 2026-02-26
Online: 2026-05-21

Impacts of Wafer Thinning Process Using Laser Slice Technique on Silicon Carbide Device Characteristics

Kyohei Akiyoshi[1,a*], Takanori Tanaka[1,b], Shunta Takahashi[2,c], Kazumasa Iwanaga[1,d], Kenichi Hamano[1,e] and Akihiko Furukawa[1,f]

[1]Power Device Works, Mitsubishi Electric Corporation, 1-1-1 Imajuku-higashi, Nishi-ku, Fukuoka, Fukuoka, 819-0192, Japan

[2]Advanced Technology R&D Center, Mitsubishi Electric Corporation, 8-1-1 Tsukaguchi-honmachi, Amagasaki, Hyogo, 661-8661, Japan

[a*]Akiyoshi.Kyohei@ea.MitsubishiElectric.co.jp, [b]Tanaka.Takanori@cb.MitsubishiElectric.co.jp, [c]Takahashi.Shunta@bp.MitsubishiElectric.co.jp, [d]Iwanaga.Kazumasa@aj.MitsubishiElectric.co.jp, [e]hamano.kenichi@df.mitsubishielectric.co.jp, [f]Furukawa.Akihiko@df.MitsubishiElectric.co.jp

Keywords: SiC wafer, reutilization process, recycling wafer, laser slice, JBS diode, MOSFET.

Abstract. A laser slicing technique is an attractive alternative to grinding for thinning SiC wafers. This method has the potential to enable the reutilization of SiC wafers and reduce the waste generated during the grinding process. This paper comprehensively investigates the technical feasibility of laser slicing for the fabrication of SiC power devices. SiC JBS samples fabricated with laser irradiation revealed that by selecting the appropriate laser conditions, we can employ the technique without adversely affecting the JBS leakage current characteristics. Additionally, we fabricated SiC MOSFETs through wafer thinning using the laser slicing technique. The key electrical characteristics of the MOSFETs, including I_{GSS}, I_{DSS}, V_{th} and $V_{DS(on)}$, showed no differences compared to those fabricated using conventional grinding. These results indicate that laser slicing is a highly promising thinning technique for the fabrication of SiC power devices.

Introduction

Silicon carbide (SiC) power devices offer superior characteristics, including high breakdown voltage, low on-resistance, low switching loss, and high-temperature operation. In their application to high-power systems, significantly improved performance is expected compared to their Si counterparts [1].

However, the manufacturing costs of SiC power devices remain high due to the high costs of SiC wafers. The high costs of SiC wafers are attributed not only to the costly sublimation bulk growth process but also to wafering processes such as slicing and grinding, which are challenging due to the inherent hardness and brittleness of SiC [2, 3]. Additionally, in the fabrication of SiC power devices, SiC wafers are thinned to enhance their performance. The conventional thinning process used today employs mechanical grinding, which removes valuable SiC material as sludge, creating a significant environmental burden.

Recently, the laser slicing technique has attracted significant attention as a method for slicing wafers from ingots [4]. Laser slicing can substantially reduce material loss (kerf loss) while maintaining high throughput [5]. In light of these advantages, the use of laser slicing for wafer thinning has been proposed as a replacement for conventional grinding. The sequence of wafer thinning process is illustrated in Fig. 1 [6]. This method enables device re-manufacturing on the wafer left after laser slicing. By applying this method to SiC power devices, it is expected to reduce manufacturing costs and decrease the environmental impact associated with SiC sludge.

A primary concern regarding the application of laser slicing for SiC wafer thinning is its potential adverse impacts on the characteristics of SiC power devices. This paper comprehensively evaluates the impacts of the laser slicing technology on device characteristics. First, we systematically

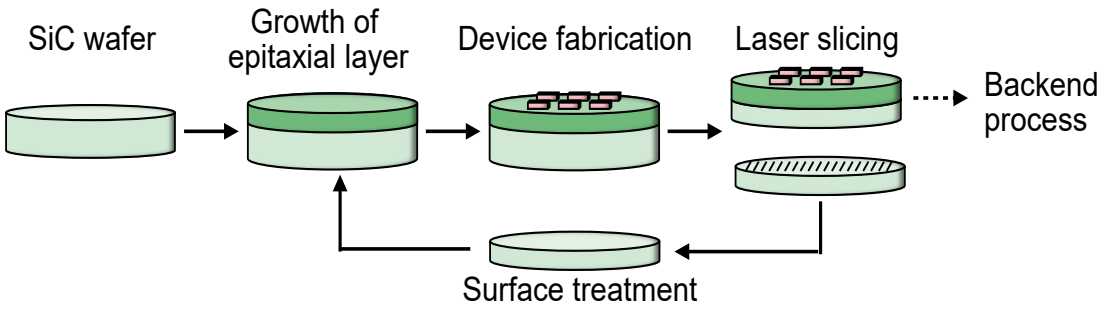

Fig. 1. An example of a wafer reutilization process applying laser slicing technology for wafer thinning.

investigate the effects of focused laser irradiation on Junction Barrier Schottky (JBS) electrodes, which are sensitive to heat. Second, we apply the laser slicing technique to the thinning process of SiC MOSFETs and present their electrical characteristics in comparison to those fabricated using conventional grinding process, demonstrating that the laser slicing is a promising technique to replace grinding.

Impacts of Laser Irradiation on JBS Electrodes

Sample Chip Preparation and Evaluation Procedure.

1200 V SiC JBS diodes were fabricated to examine the impacts of laser slicing. The schematic top view and 3D cross-sectional view of the sample JBS diode, along with the fabrication and evaluation flow of the JBS diodes, are shown in Fig. 2 and 3. An epitaxial layer was grown on the Si-face of a 6-inch N-type 4H-SiC substrate with a 4° off-cut angle, and a JBS structure was formed on this epitaxial layer. Using a laser slicing apparatus, the laser beam was irradiated to the SiC wafer from the backside (C-face), focusing it at the desired depth from the JBS electrodes. The focused laser beam was scanned along a line depicted in Fig. 2, generating a modified layer and line-shaped cracks within the wafers. The laser power was set at 2.5 W, 5.0 W, and 7.5 W, and the distance between the laser focal point and the surface electrode was varied from 20 μm to 160 μm in 20 μm increments. Finally, a backside metal electrode was formed on the C-face, and the wafer was diced into sample JBS chips.

We measured the reverse characteristics (leakage current) of the sample JBS diodes as an indicator sensitive to the heat generated by laser irradiation. For samples exhibiting increased leakage current, emission microscopy (EMS) was employed from the backside of the samples. Using EMS, we can detect light emissions from current leakage points, allowing us to pinpoint the defective locations. After removing the anode and Schottky barrier electrodes (Ti), scanning electron microscopy (SEM) observation was performed to assess the surface morphology, followed by energy-dispersive X-ray spectroscopy (EDX) conducted at the leakage points.

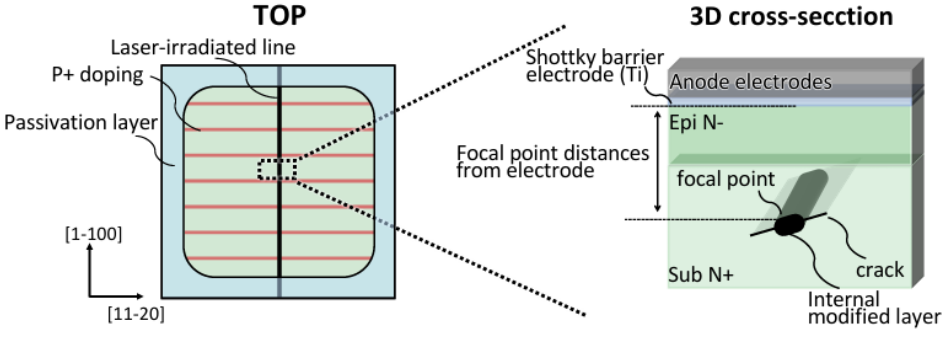

Fig. 2. (a) Top view and (b) 3D cross-sectional view of the fabricated 1200 V JBS diode.

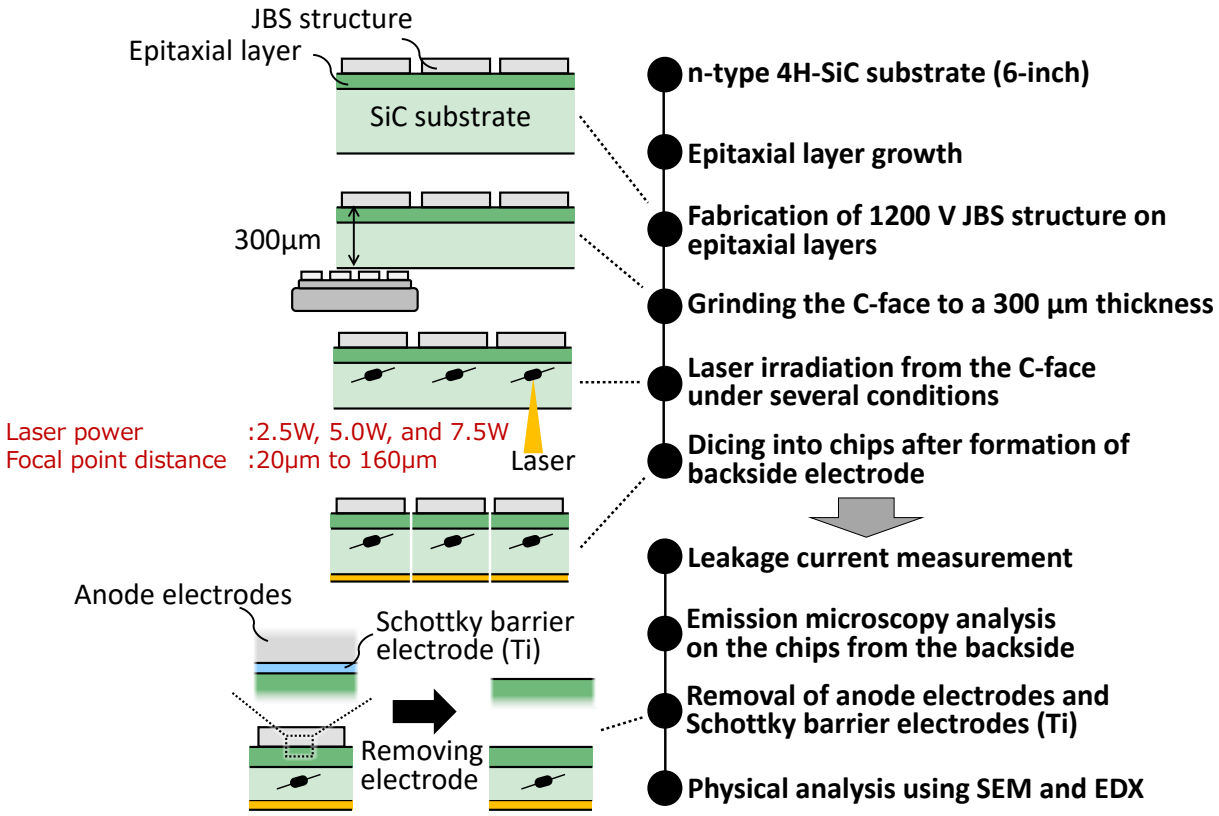

Fig. 3. Fabrication and evaluation process flow of 1200 V JBS diodes.

Leakage Current Measurement and Analysis.

The reverse characteristics of the fabricated JBS diodes under laser power of 2.5 W, 5.0 W and 7.5 W are shown in Fig. 4(a), (b) and (c), respectively. At 2.5 W, all the chips exhibited I-V curves almost identical to that without laser irradiation. At 5.0 W and 7.5 W, the chips with the focal point distances ranging from 60 μm to 140 μm also exhibited I-V curves comparable to that without laser irradiation. In contrast, increase in leakage current was observed for the samples with shorter focal point distances and higher laser power.

To clarify the relationship between the increase in leakage current and laser irradiation to the JBS diodes, EMS analysis was performed on the defective chips with leakage current. The light emission was clearly observed from the backside when the leakage current flew over around 10 μA. Optical and EMS images and the I-V curve taken during EMS analysis of the sample are shown in Fig. 5(a), (b), and (c). The laser irradiation conditions for this sample are a laser power of 5.0 W and a focal point distance of 40 μm. In Fig. 5(b), the dark line indicates the modified layer with internal cracks generated by the laser irradiation. At the center of the line (just above the laser focus scanning line),

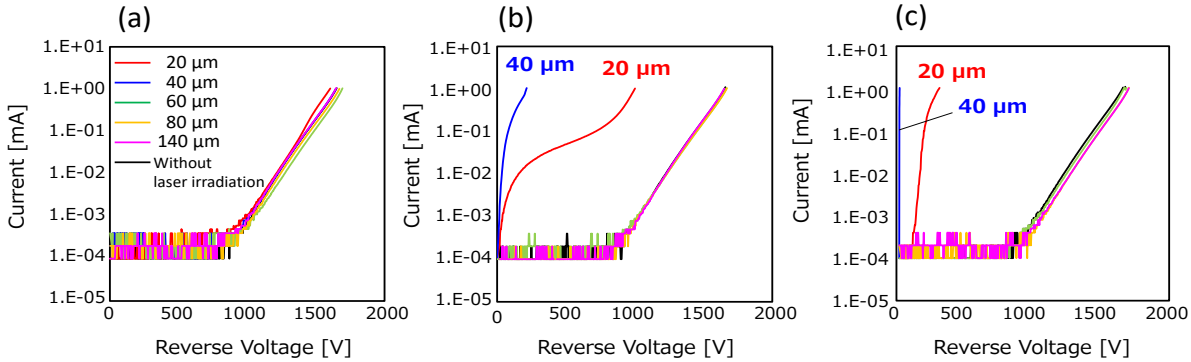

Fig. 4. Reverse characteristics of 1200 V JBS diodes with irradiated laser power at (a) 2.5 W, (b) 5.0 W, and (c) 7.5 W.

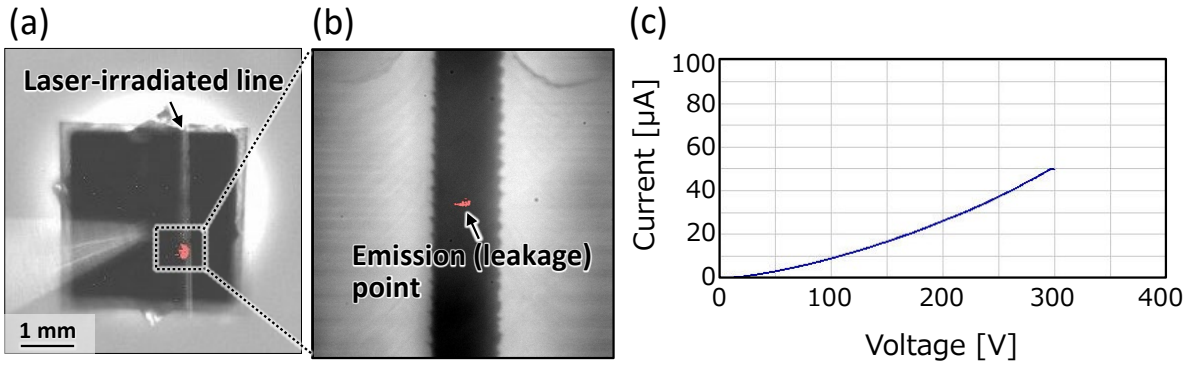

Fig. 5. (a) Optical + EMS image of JBS with leakage current, (b) an enlarged view of the emission point in (a), and (c) I-V characteristics during the EMS analysis. Laser slicing for the sample was performed under a laser power of 5.0 W and a focal point distance of 40 μm.

an emission is clearly visible when the leakage current flows. This result suggests that the laser irradiation is the direct cause for the pinpoint leakage current. To reveal the mechanism by which leakage current occurred, we examined JBS surfaces after etching electrodes. Fig. 6(a) shows an optical image of the JBS diode surface that is subjected to laser irradiation at a power of 7.5 W and a laser focal point distance from the surface of 20 μm. Cracks are visible inside the wafer along the line where the laser beam was scanned. Fig. 6(b) and (c) show SEM images of the chip edge and JBS area of the sample, respectively. It should be noted that there is no Ti deposition in the chip peripheral area shown in Fig. 6(b). Although no laser-induced melting marks are observed in Fig. 6(b), small melting marks are observed just on the laser irradiated point in Fig. 6(c). EDX spectra at the points, melting marks (i) and non-melting marks (ii), in Fig. 6(c) are shown in Fig. 7. EDX analysis revealed that detectable Ti exists exclusively at the melting marks after removal of the Ti electrode. This indicates that the melting marks are alloys including Ti, and that the presence of the Ti is a key factor to the formation of these melting traces, which generate leakage current paths.

To investigate the parameter range where melting traces, specifically current leakage points, are created, we systematically examined the sample surfaces after stripping the electrodes. The surface

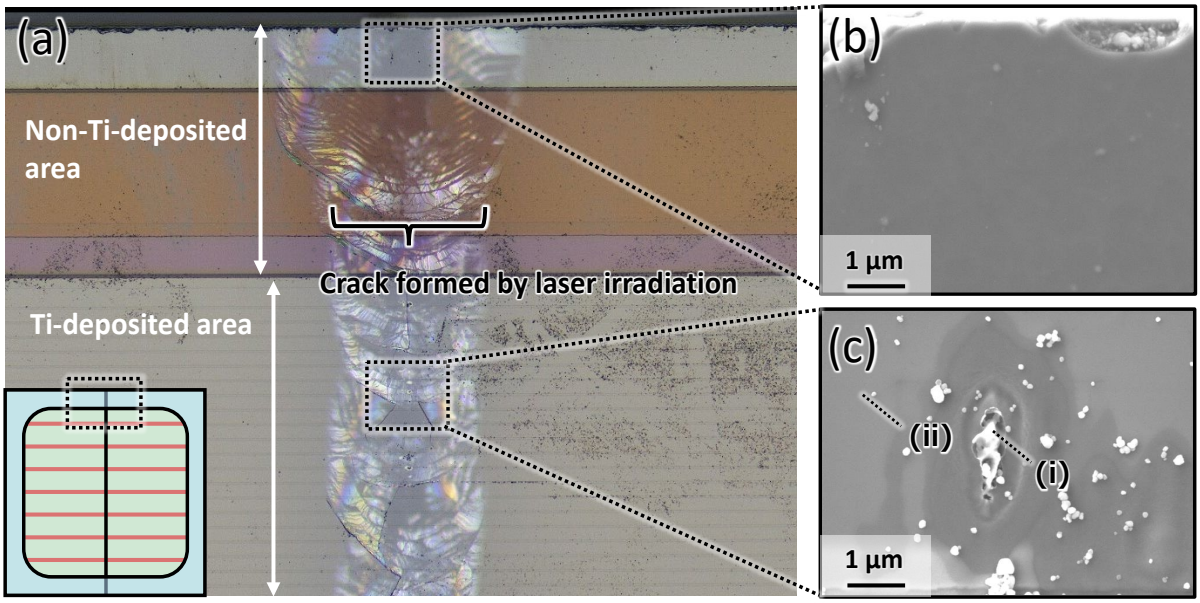

Fig. 6. (a) An optical image of the sample JBS chip after the removal of electrodes. Inner cracks are visible along the laser-irradiated line. (b) A SEM image of the chip edge including the laser-irradiated line. No melting marks are present in the area. (c) A SEM image of the surface in JBS area. Melting marks are visible on the laser-irradiated line. A laser power and a focal point distance from the Ti electrode are 7.5W and 20 μm.

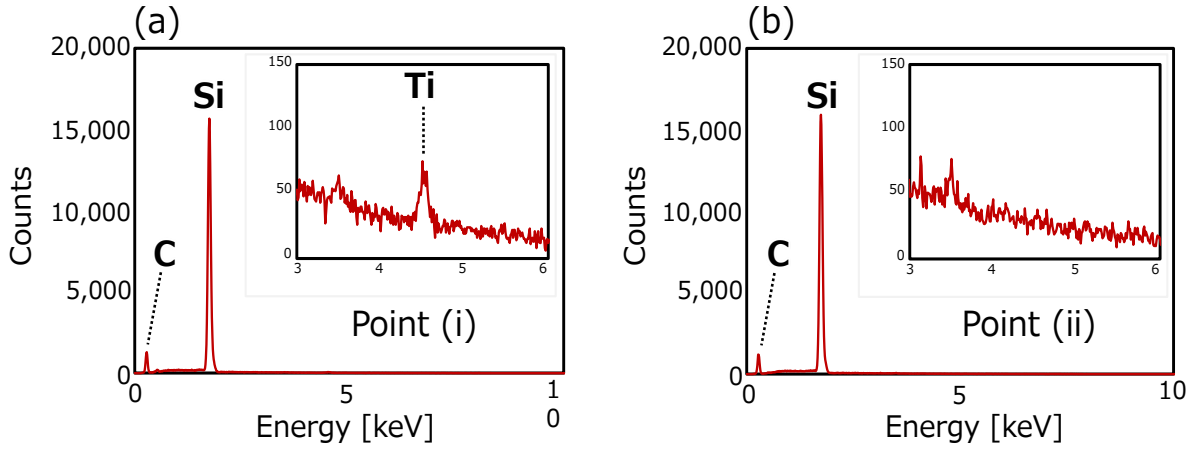

Fig. 7. EDX spectrum at the points indicated in Fig. 6(c): (a) melting marks (i) and (b) non-melting marks (ii).

images of the JBS diodes observed by SEM are shown in Fig. 8. Melting traces were observed on the SiC surface directly above the laser irradiation line. It was found that the higher the laser power and the shorter the distance from the electrodes the larger the area of the melting trace tended to be.

Based on these results, we take the discussion a step further. When the Ti electrode does not exist, no trace was observed (Fig. 6(b)). This means that Ti electrodes absorb the laser light effectively, and it is converted to heat. As indicated in Fig. 7, Ti is detected in and around the melting traces. It is known that SiC and Ti can react to form silicide and the silicide formation can occur at relatively low temperatures (below 1100°C [7]) compared to Ti melting point of 1668°C, suggesting that the formation of alloy makes it easier to form melting marks. Fig. 9 schematically illustrates how melting marks are formed above laser focal points.

From Fig. 4, it is evident that no significant impact on electrical characteristics was detected when the focal point distance from the electrode exceeded 60 µm. Considering that the typical final wafer thickness for power devices is more than around 100 µm, it is possible to establish the laser irradiation conditions for laser slicing that does not affect device characteristics.

Application of Laser Slicing to SiC MOSFETs

Laser slicing was applied to the thinning of 1200 V SiC MOSFETs. The fabrication process flow for SiC MOSFETs is shown in Fig. 10. An epitaxial layer was grown on the Si-face of a 6-inch N-type 4H-SiC substrate with a 4° off-cut angle, and a MOSFET structure was fabricated on it. Using a laser slicing apparatus, the laser beam was irradiated and focused inside the SiC wafer from the backside (C-face) at a depth of 140 µm from the MOSFET surface. The laser beam was scanned over the entire wafer, forming a modified layer and cracks inside the wafer. Then the wafer was split into two pieces. Images of the wafers observed from the top side before and after laser slicing are shown in Fig. 11(a), (b) and (c). No middle or large size defects such as cracks or chippings are visible on the laser-sliced wafers. The detached surfaces were subsequently ground to achieve a final thickness of 100 µm. Finally, a backside metal electrode was formed, and the wafer was diced into chips.

The main electrical characteristics of the MOSFETs, including the gate leakage current (I_{GSS}), the threshold voltage (V_{th}), the drain leakage current at 1200 V (I_{DSS}), and the on-voltage ($V_{DS(ON)}$), were measured. The results are shown in Fig. 12(a), (b), (c), and (d). The electrical characteristics of the MOSFETs thinned by the laser slicing process are compared to those thinned by the conventional grinding process. The I_{GSS} remains very low for the laser-processed MOSFETs and the threshold voltage V_{th} shows no significant change compared to MOSFETs thinned by conventional grinding, indicating that the gate oxide film was not damaged by the laser irradiation. Furthermore, no significant changes, including standard deviation, are observed for the I_{DSS}. The $V_{DS(ON)}$ also shows no significant change, suggesting that the laser slicing process does not damage the drift layer or electrode. Overall, we observe no adverse impacts on MOSFET characteristics due to the laser slicing.

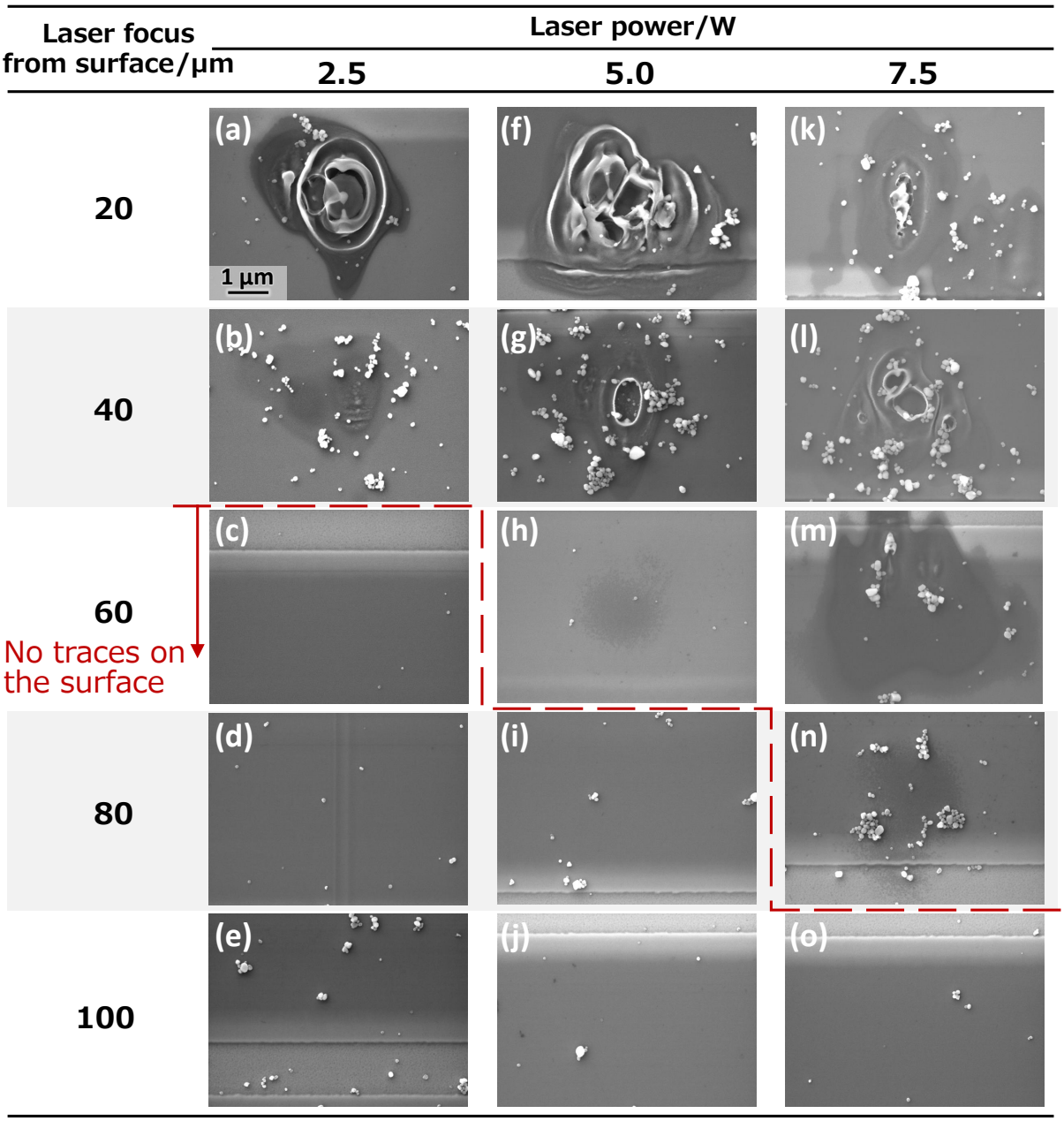

Fig. 8. SEM images of the JBS sample surface on the laser-irradiated line with various laser conditions ((a)-(o)) after the removal of anode electrodes and Schottky barrier electrodes (Ti).

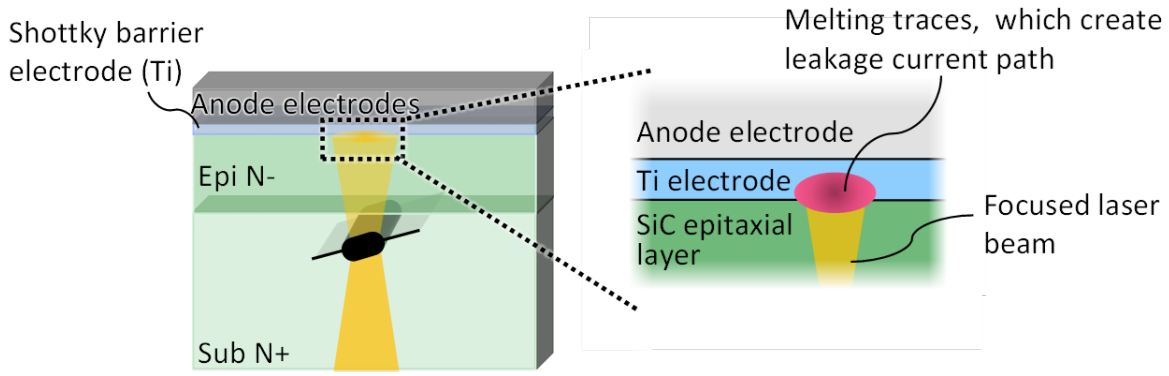

Fig. 9. Illustrative diagram depicting the impact on electrodes due to laser light irradiation during laser slicing.

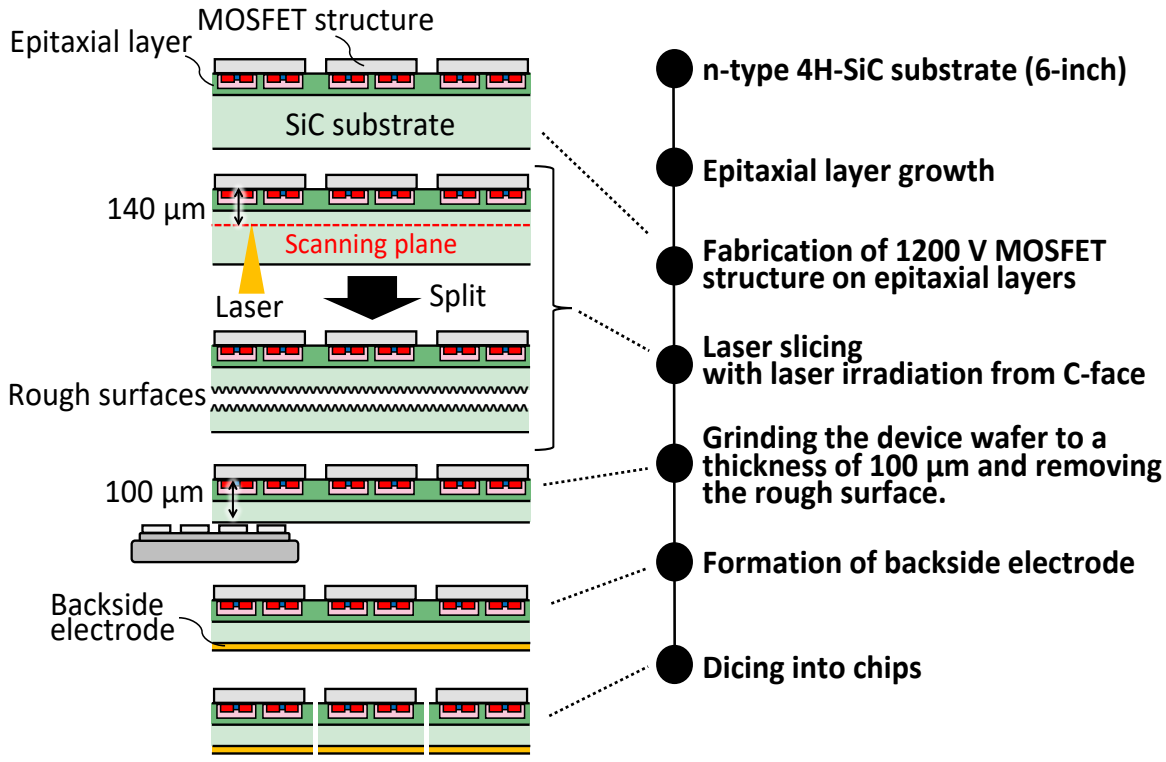

Fig. 10. 1200V MOSFET fabrication process flow.

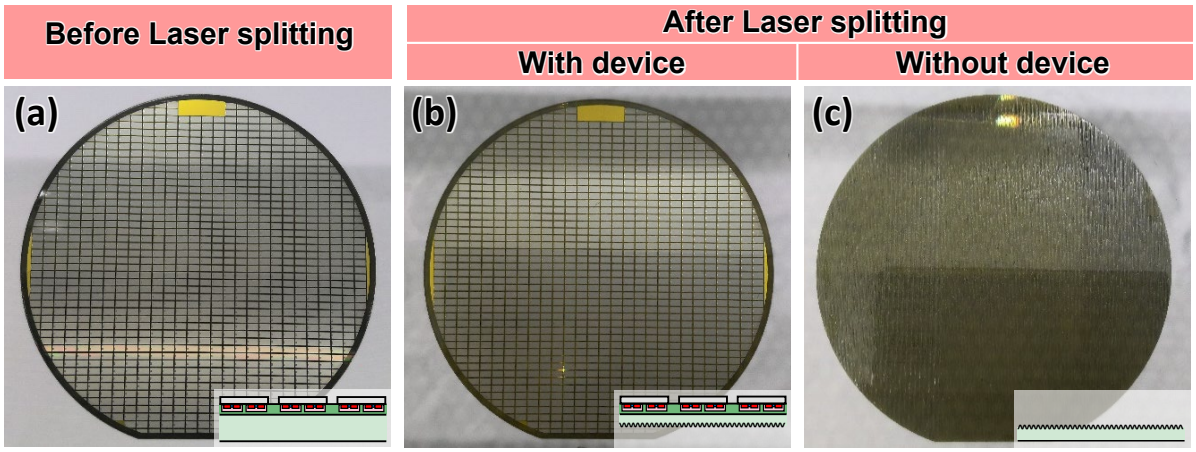

Fig. 11. Top surface images of wafers: (a) before laser slicing, (b) with device structures after laser slicing, and (c) without device structures after laser slicing.

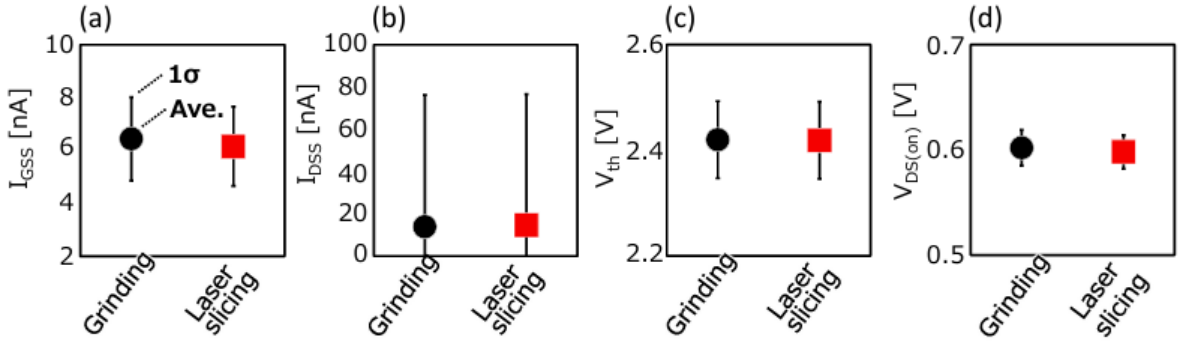

Fig. 12. Comparison of the main electrical characteristics ((a) I_{GSS}, (b) V_{th}, (c) I_{DSS}, and (d) $V_{DS(ON)}$) of the MOSFETs thinned by laser slicing and grinding only. Error bars represent $\pm 1\,\sigma$.

Summary

We investigated the laser slicing technique as an alternative to grinding for thinning SiC wafers. The impacts of focused laser light onto the SiC wafers were examined using test devices with JBS electrodes, whose characteristics are sensitive to heat. Measurements of leakage current revealed that higher laser power and shorter distances between the laser focus and JBS electrodes (below 60 μm) increased leakage current. SEM observation and EMS analysis revealed that the heat from the laser beam creates melting traces on the SiC surface, generating leakage current paths. However, these results suggest that by selecting the appropriate laser irradiating parameters, laser slicing can be applied to the fabrication of SiC power devices. Based on our findings, SiC MOSFETs were experimentally fabricated utilizing the laser slicing technique. The performance of the MOSFETs exhibited no significant differences when compared to those fabricated using the conventional grinding technique. These results demonstrate that the laser slicing is a promising SiC wafer thinning technique replacing grinding.

References

[1] T. Kimoto, Jpn. J. Appl. Phys., **54**, 040103 (2015).

[2] X. Yu, W. Wu, B. Li, X. Xiu, Y. Zheng, and R. Zhang, Appl. Surf. Sci., **697**, 163014 (2025).

[3] G. Shang, H. Wang, H. Huang, and R. Kang, Int. J. Mech. Sci., **247**, 108147 (2023).

[4] Y. Lu, X. Li, B. Chen, X. Zhang, X. Li, Y. Wang, Y. Chen, M. Wang, and S. Wang, Opt. Express, **33**(16), 33456 (2025).

[5] K. Hirata, Proc. of SPIE, **10520**, 1052003 (2018).

[6] T. Ishida, T. Ushijima, S. Nakabayashi, K. Kato, T. Koyama, Y. Nagasato, J. Ohara, S. Hoshi, M. Nagaya, K. Hara, T. Kanemura, M. Taki, T. Yui, K. Hara, D. Kawaguchi, K. Kuno, T. Osajima, J. Kojima, T. Uesugi, A. Tanaka, C. Sasaoka, S. Onda, and J. Suda, Appl. Phys. Express, **17**, 026501 (2024).

[7] A. Martychowiec, N. Kwietniewski, K. Kondracka, A. Werbowy, and M. Sochacki, Proc. of SPIE, **11581**, 115810W (2020).